

Pressure-induced amorphization and metallization in orthorhombic SiP

Qiru Zeng(曾琪茹), Youjun Zhang(张友君), Yukai Zhuang(庄毓凯), Linfei Yang(杨林飞), Qiming Wang(王齐明), and Yi Sun(孙熠)

Citatio: Chin. Phys. B, 2025, 34 (**9**): 096102. DOI: 10.1088/1674-1056/add4f6
http://cpb.iphy.ac.cn; http://iopscience.iop.org/cpb

What follows is a list of articles you may be interested in

First-principles study on structural, electronic, and superconducting properties of Laves-phase alloy $HfZn_2$ under pressure

Xiao Ma(马晓), Tao Wang(王涛), Jianfeng Wen(文剑锋), Zhenwei Zhou(周振玮), and Hongyu Zhu(朱红玉)
Chin. Phys. B, 2025, 34 (**8**): 086108. DOI: 10.1088/1674-1056/ade5a1

Pressure-induced structural transitions and metallization in $ZrSe_2$

Yiping Gao(高一平), Chenchen Liu(刘晨晨), Can Tian(田灿), Chengcheng Zhu(朱程程), Xiaoli Huang(黄晓丽), and Tian Cui(崔田)
Chin. Phys. B, 2024, 33 (**12**): 126104. DOI: 10.1088/1674-1056/ad8ec9

Impact of incident direction on neutron-induced single-bit and multiple-cell upsets in 14 nm FinFET and 65 nm planar SRAMs

Shao-Hua Yang(杨少华), Zhan-Gang Zhang(张战刚), Zhi-Feng Lei(雷志锋), Yun Huang(黄云), Kai Xi(习凯), Song-Lin Wang(王松林), Tian-Jiao Liang(梁天骄), Teng Tong(童腾), Xiao-Hui Li(李晓辉), Chao Peng(彭超), Fu-Gen Wu(吴福根), and Bin Li(李斌)
Chin. Phys. B, 2022, 31 (**12**): 126103. DOI: 10.1088/1674-1056/ac785a

Mechanisms of atmospheric neutron-induced single event upsets in nanometric SOI and bulk SRAM devices based on experiment-verified simulation tool

Zhi-Feng Lei(雷志锋), Zhan-Gang Zhang(张战刚), Yun-Fei En(恩云飞), Yun Huang(黄云)
Chin. Phys. B, 2018, 27 (**6**): 066105. DOI: 10.1088/1674-1056/27/6/066105

High-pressure structural properties of tetramethylsilane

Zhen-Xing Qin(秦振兴) and Xiao-Jia Chen(陈晓嘉)
Chin. Phys. B, 2016, 25 (**2**): 026104. DOI: 10.1088/1674-1056/25/2/026104

Pressure-induced amorphization and metallization in orthorhombic SiP

Qiru Zeng(曾琪茹)[1], Youjun Zhang(张友君)[1], Yukai Zhuang(庄毓凯)[1], Linfei Yang(杨林飞)[2], Qiming Wang(王齐明)[1,†], and Yi Sun(孙熠)[2,‡]

[1] *Institute of Atomic and Molecular Physics, Sichuan University, Chengdu* 610065, *China*
[2] *School of Materials Science and Engineering, Jingdezhen Ceramic University, Jingdezhen* 333403, *China*

(Received 16 February 2025; revised manuscript received 28 April 2025; accepted manuscript online 7 May 2025)

Amorphous states of two-dimensional (2D) materials frequently exhibit remarkable physical properties that differ significantly from their crystalline counterparts. Typically, metastable amorphous states can be achieved through rapid quenching from high temperatures. However, the heating process is detrimental to the structural integrity of 2D materials. In this study, we successfully utilized pressure as an external stimulus to induce an amorphous state in layered crystal SiP. Comprehensive experimental and theoretical investigations revealed metallization in the high-pressure amorphous phase of SiP. The recovered samples were characterized using x-ray diffraction, Raman spectroscopy, high-resolution transmission electron microscopy, and selected area electron diffraction. The results indicate that the metallic amorphous SiP obtained under extreme conditions can be stabilized at ambient conditions. These findings provide a viable pathway for inducing metastable phases in 2D materials and offer new insights into the design and development of advanced electronic devices.

Keywords: crystal-to-amorphous transition, metallization, layered semiconductors, high pressure

PACS: 61.43.Dq, 85.40.Ls, 72.20.–i, 91.60.Hg

DOI: 10.1088/1674-1056/add4f6 **CSTR:** 32038.14.CPB.add4f6

1. Introduction

Since the successful synthesis of graphene, extensive research has been conducted to explore novel two-dimensional (2D) materials with highly tunable electronic and optoelectronic properties, as well as their potential applications. To date, multiple remarkable properties have been discovered in 2D materials, such as metallization, superconductivity, and ferroelectricity.[1–4] Compared to the crystalline forms of 2D materials, substantially less research attention has been devoted to their amorphous counterparts. In some cases, the highly disordered forms showed strange physical effects that were different from their stable state. This made them interesting candidates for fields like optoelectronics, energy storage, and catalysis.[5–7] A case in point is amorphous MoS_2, which has higher activity in hydrogen evolution reaction (HER) catalysis than that of its crystalline phase.[8,9] The primary objective is to develop a method for controllably switching between amorphous and crystalline phases, leveraging the distinct properties of each phase.

Traditionally, the metastable amorphous materials can be acquired by virtue of quick quenching from a high temperature. However, such a rapid heating-cooling path can only inherit the intrinsic properties of high-temperature phases.[10,11] And moreover, the heating process at times might damage materials that are vulnerable to high temperature (*e.g.*, decomposition reaction). Very recently, a new method named the supercritical carbon dioxide (SC CO_2) assisted process has been successfully applied in the fabrication of 2D amorphous materials, but this strategy involved a complicated processing procedure and, in the meantime, inevitably introduced external impurities.[12–15] As such, it is imperative to call for an alternative way to achieve amorphization in 2D materials.

Pressure is a clean and effective method to alter atomic arrangements, potentially disrupting the crystal structure entirely, a process known as amorphization. Pressure-induced amorphization (PIA) is regarded as an important condensed matter phenomenon, which was first discovered in ice.[16,17] Subsequently, PIA was observed in many other materials, such as silicon Si,[18,19] α-quartz SiO_2,[20] VO_2,[21] TiO_2,[22] and boron carbide B_4C.[23] The amorphous 2D materials display exceptional properties which are significantly unique compared to their crystalline counterpart, PIA has become a very interesting area of study. These differences pave the way for new physical phenomena and innovative applications.

As an important 2D layered semiconductor material,[24] SiP is a medium bandgap semiconductor with an energy gap ranging approximately from 1.69 eV to 2.59 eV.[25,26] This property enables efficient photoelectric conversion across a wide range of wavelengths. SiP also has great linear optical properties and low crystal symmetry,[24,27,28] making it

†Corresponding author. E-mail: qmwang@scu.edu.cn
‡Corresponding author. E-mail: sunyi@jcu.edu.cn

© 2025 Chinese Physical Society and IOP Publishing Ltd. All rights, including for text and data mining, AI training, and similar technologies, are reserved.

suitable for applications such as polarization-sensitive photodetectors, angle-dependent electronics, and synaptic devices in various fields. Currently, the study of SiP under extreme conditions has not been thoroughly explored. Chen *et al.*[29] investigated the structural evolution of SiP under pressure through synchrotron x-ray diffraction (XRD) experiments. They revealed a pressure-induced irreversible amorphization at 26.1 GPa, evidenced by a broad diffuse background and the loss of major Bragg peaks. In this work, we systematically investigate the high-pressure structural phase transitions and electronic property evolution of SiP through Raman spectroscopy, XRD, high-resolution transmission electron microscope (HRTEM), selected area electron diffraction (SAED), and conductivity measurement experiments, combined with first principles calculations. The mechanism of the irreversible amorphization was explored comprehensively by the experimental and theoretical methods. We also found that an irreversible metallization was induced by the irreversible amorphization.

2. Experimental methods

SiP powder, with a purity of 99.99%, was acquired from Nanjing Mako Nano Technology Company. This material belongs to the category of 2D layered materials.[26,30] The XRD data were collected at room temperature and ambient pressure utilizing a Rigaku Ultima IV Powder x-ray diffractometer, which is equipped with a rotating anode target (Cu $K\alpha$, $\lambda = 1.5406$ Å). The structural parameters were refined using the GSAS software package.[31]

The high-pressure Raman measurements at room temperature were conducted at Center for High Pressure Science and Technology Advanced Research (HPSTAR). The experimental setup was employed in a diamond anvil cell (DAC) with anvil culet sizes of 300 μm and stainless steel gaskets for encapsulation.[32] No pressure-transmitting medium was introduced into the chamber. The pressure calibration was performed using the ruby fluorescence spectrum.[33] Prior to the experiment, system calibration was performed using a Si wafer. Raman spectra were obtained using an argon laser with a spectral resolution of 1.0 cm^{-1}, covering the range of 100 cm^{-1}–700 cm^{-1}.

Microscopic structural and morphological analyses of the sample were performed using HRTEM and SAED operated at an accelerating voltage of 100 kV.[34] HRTEM was employed to acquire high-resolution and high-magnification micrographs of the 2D semiconductor SiP. In parallel, SAED was utilized to investigate the crystal structure and associated characteristics through the analysis of diffraction patterns.

The XRD experiments for both the initial and recovered samples were performed at beamline 15U1 of the Shanghai Synchrotron Radiation Facility ($\lambda = 0.6199$ Å) at room temperature and pressure. The spot sizes were ~ 3.1 μm×2.9 μm. The sample–detector distance and geometric parameters were calibrated using CeO_2 standard. The average acquisition time was 60 s for each experiment.

The high-pressure *in situ* conductivity measurement experiment was conducted in the DAC using the van der Pauw method.[35] The design for DAC conductivity measurements is shown in Fig. 1. The Keithley 6221 DC and AC constant current source and the Model 2182A nanovoltmeter were used to check the sample's voltage and current. The resistance value was ultimately derived based on the van der Pauw method, and the experiment was repeated 3–5 times.[36] The temperature-dependent electrical conductivity of SiP under varying pressures was systematically investigated in a liquid nitrogen environment.

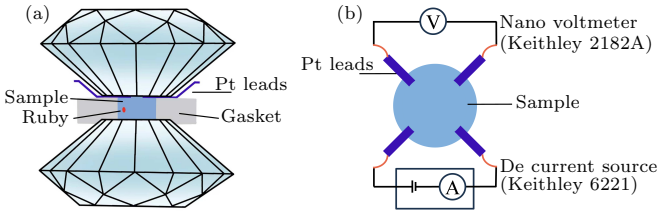


Fig. 1. Experimental diagram of sample assembly for high-pressure conductivity measurement. (a) Schematic diagram of conductivity measurement using the four-electrode method in a DAC. (b) Diagram of the sample arrangement. The sample is a disc approximately 80 μm in diameter, with four platinum (Pt) leads attached to it. The sample chamber is constructed with a pre-indented stainlesssteel gasket, insulated with cubic boron nitride (CBN), and contains both a ruby marker and the sample within its interior. There is no pressure-transmitting medium present in the sample chamber. The pressure inside the sample chamber was determined by the ruby fluorescence wavelength positioned within the chamber.

First-principles calculations were carried out based on density functional theory (DFT) using the Vienna *Ab Initio* Simulation Package (VASP).[37,38] The Perdew–Burke–Ernzerhof (PBE) method was used in the generalized gradient approximation (GGA) as the exchange–correlation functional.[39–41] After the structural relaxation was done, the HSE06 hybrid functional was used to recalculate the electronic states and density of the band structure.[42]

3. Results and discussion

3.1. X-ray diffraction

SiP possesses a layered structure owing to van der Waals (vdW) forces and is classified as the $Cmc2_1$ group at room environment.[29] The XRD refinement results of SiP, recorded under ambient temperature and pressure, are presented in Fig. 2. It shows that the experimental data align well with the theoretical values, with an R_{WP} of approximately 9.49%. The corresponding lattice parameters are $a = 3.61(28)$ Å, $b = 20.45(14)$ Å, $c = 13.64(8)$ Å. The layered structure of SiP is illustrated in the inset diagram of Fig. 2. Three phosphorus (P) atoms and four silicon (Si) atoms are interconnected

through covalent bonding, with each P atom forming three Si–P bonds with neighboring Si atoms. This bonding configuration describes the atomic arrangement within a single layer of SiP. Multilayer SiP is subsequently constructed by stacking these single layers along the *c*-axis, with the layers aligned in the *ab* plane.

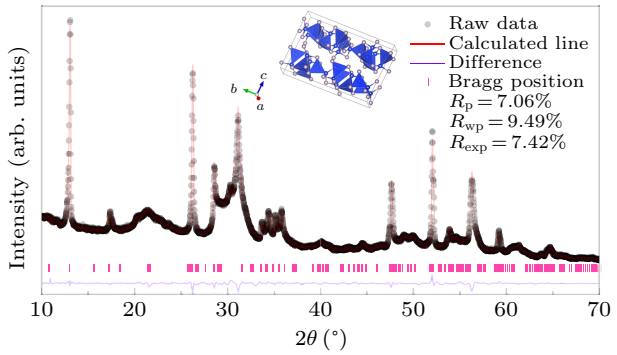


Fig. 2. XRD refinement of SiP at ambient temperature and pressure, SiP exhibits an orthorhombic structure. The insert diagram shows a schematic representation of the SiP layered structure, where silicon (Si) atoms are depicted in blue and phosphorus (P) atoms in gray.

3.2. Pressure-dependent Raman spectroscopy

Raman spectroscopy is widely recognized as an important technique for characterizing materials and studying phase transitions, particularly through the appearance or disappearance of lattice vibrational modes.[43–45] Here, Raman spectroscopy was employed to further investigate the properties of SiP under high pressure.

The phonon vibration modes of SiP can be decomposed into $\Gamma_{\text{Raman}} = 24A_1 + 12A_2 + 12B_1 + 24B_2$.[46] Among the different modes, only the modes in the *ab*-plane are detectable.[46] Consequently, the primary active vibration modes in this system are A_1 and A_2, all of which correspond to in-plane vibrations. The Raman spectrum of SiP at room temperature and atmospheric pressure is presented in Fig. 3. The Raman peak positions measured in this study show excellent agreement with the previous report.[47]

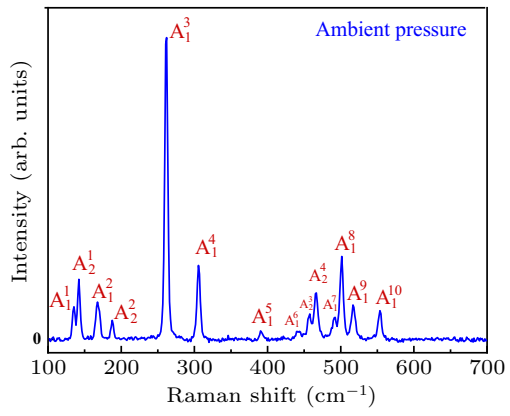


Fig. 3. Raman vibrational spectroscopy measurements of SiP with the range of 100 cm^{-1}–700 cm^{-1} at room temperature and atmospheric pressure. The Raman-active modes are identified as A_1 and A_2 modes, as indicated in red.

The evolution of Raman spectra of SiP was shown in Fig. 4. To facilitate the discussion, we divided the analysis of the high-pressure Raman spectra into three parts: (i) Raman shift increases significantly with varying pressure. (ii) Between 6.1 GPa and 12.1 GPa, the peaks A_1^2 (167.6 cm^{-1}), A_2^3 (440.9 cm^{-1}), A_1^7 (490.1 cm^{-1}), and A_1^8 (516.7 cm^{-1}) disappear accompanied by the emergence of new peaks of P_1 at 115.1 cm^{-1} and P_2 at 163. cm^{-1}. Additionally, two new peaks (marked as P_3 and P_4) appear at 12.1 GPa. These changes in vibrational modes may be caused by lattice distortion introduced by pressure. Interestingly, this phenomenon likely correlates with the changes in electronic structure. We will investigate this further by measuring the conductivity at high pressures. (iii) At 23.3 GPa, the Raman peak exhibits significant Raman peak broadening, indicating the loss of long-range structural order due to pressure-induced amorphization. Upon releasing the pressure, the Raman spectra exhibit no noticeable changes, indicating that the structural transition is irreversible.

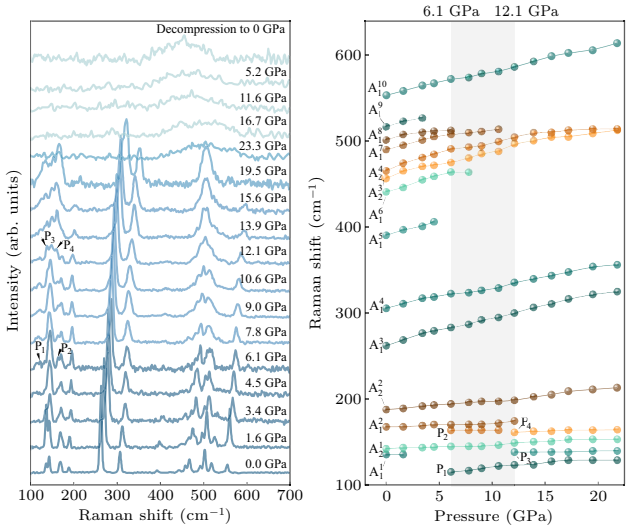


Fig. 4. (a) Raman spectra of SiP measured during compression and decompression. The arrows marked as P_1, P_2, P_3, P_4 representing the occurrence of the newly observed peak. (b) Raman frequency of SiP shifts with varying pressure. The gray shaded region was highlighted to facilitate the observation of peak emergence and disappearance.

3.3. XRD, HRTEM, and SAED analyses of the recycled samples

In order to reveal the structural evolution of SiP more clearly, we performed HRTEM, SAED, and XRD analyses on the pristine samples and samples recovered from 23.3 GPa. The XRD pattern of pristine SiP (Fig. 5(a)) displays sharp Bragg peaks, and the corresponding HRTEM image (Fig. 5(b)) shows a layered structure with ~ 0.301-nm interlayer spacing. The SAED pattern (Fig. 5(c)) displays sharp diffraction spots, demonstrating the high crystallinity of pristine SiP. These complementary results from XRD, HRTEM, and SAED conclusively demonstrate the layered crystal structure of the pristine SiP samples.

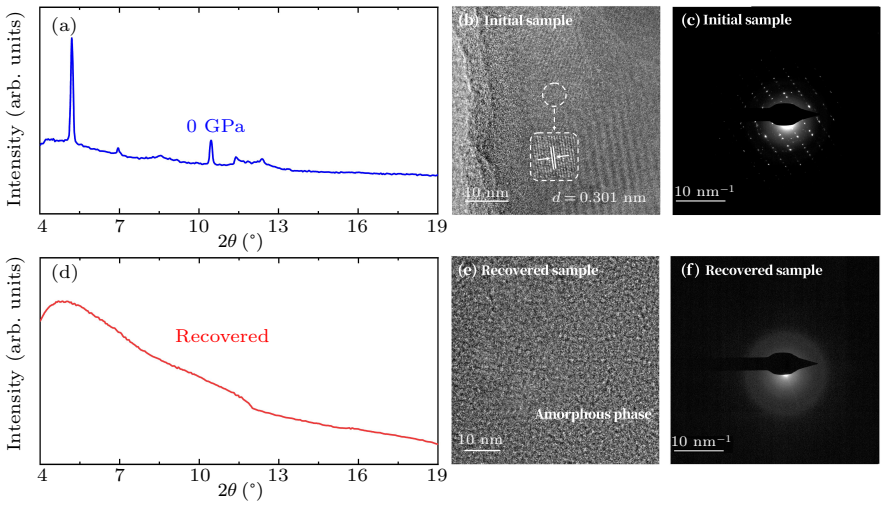


Fig. 5. Panels (a) and (d) are XRD patterns of the initial and high-pressure recovered samples. Panels (b) and (e) are HRTEM images of the initial SiP under ambient pressure and the recovered sample from approximately 23.3 GPa. Scale bars are 10 nm. Panels (c) and (f) are SAED images of the initial and recovered samples.

In contrast, structural analysis of the recovered SiP samples indicates irreversible amorphization. The XRD pattern (Fig. 5(d)) shows the disappearance of Bragg diffraction peaks, while the HRTEM of image (Fig. 5(e)) reveals an amorphous phase. The SAED pattern (Fig. 5(f)) of the recovered sample displays characteristic diffuse rings with the complete absence of Bragg diffraction spots. Collectively, these results provide unambiguous evidence for the irreversible long-range disorder in SiP under high pressure.

The Raman spectroscopy results indicate that the lattice structure of the material is significantly affected by stress under high pressure, with a transition from crystalline to amorphous occurring at approximately 23.3 GPa. This conclusion is supported by HRTEM and SAED analysis, which confirm that SiP transforms into an amorphous state upon exceeding the critical pressure. Besides, this amorphous state remains stable at ambient conditions. In general, the pressure-induced amorphization is typically explained through pressure-dependent activation energy barrier models.[48] The thermodynamic driving force provided by pressure fails to surmount the high activation energy barriers required for crystalline ordering, thereby stabilizing a kinetically trapped amorphous state. The phenomenon of pressure-induced amorphization can also observed in materials like Bi_2Se_3 and α-As_2Te_3.[49–51]

3.4. Electrical conductivity and electronic structures

In-situ high-pressure conductivity measurements were conducted up to 62.2 GPa at room temperature. As shown in Fig. 6(a), a gradual increase in conductivity with rising pressure when the pressure is low. A sudden increase in electric conductivity was observed around ~ 6.8 GPa, which could be ascribed to a structural distortion triggered by pressure. This phenomenon is largely consistent with the findings from Raman spectroscopy data. Between 6.8 GPa and 20.5 GPa, the conductivity shows a dramatic increase as compression progresses. This substantial rise in conductivity indicates that a metallization process is occurring within the material. When pressure exceeds 40.8 GPa, the conductivity remains largely unchanged with further increases in pressure, suggesting that the metallization process is complete within the sample. Notably, upon releasing the pressure back to atmospheric levels, the conductivity remained unchanged, manifesting an irreversible transition. Similar irreversible metallization behavior has been observed in other materials, such as $HfTe_2$, Sb_2Se_3, $ZrSe_2$, and certain compounds within the Sr–Ge system.[52–56]

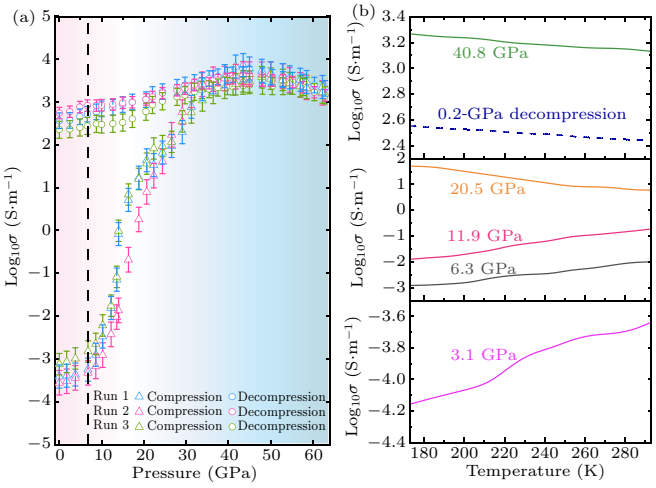


Fig. 6. (a) Pressure-induced variation of electrical conductivity of SiP. Green, pink, and blue correspond to the data from the first, second, and third compression–decompression experiments, respectively. The black vertical line signifies that the electrical conductivity begins to increase significantly at around 6.8 GPa. The error bar for conductivity determination is approximately ±10%, arising from uncertainties in both the measured resistance values and the geometric relationship between the electrode contact length and sample diameter (van der Pauw 1958). (b) The temperature dependence of the conductivity of SiP at high pressure. The irreversible decrease in electrical conductivity upon decompression to 0.2 GPa is highlighted by the blue curve.

To further validate the metallic behavior of SiP at high pressure, the temperature-dependent conductivity measure-

ments were conducted in the DAC, as shown in Fig. 6(b). According to conventional solid-state theory, the conductivity of semiconductors typically increases with temperature due to enhanced carrier density. In contrast, the conductivity of metals decreases with rising temperature because of increased electron-phonon scattering.[57,58] At 3.1 GPa, the positive relationship between conductivity and temperature showed the semiconducting behavior of SiP. However, beyond 20.5 GPa, a negative temperature coefficient of conductivity was seen, which means the material is metallic. It still exhibits a metallic state when the pressure is released.

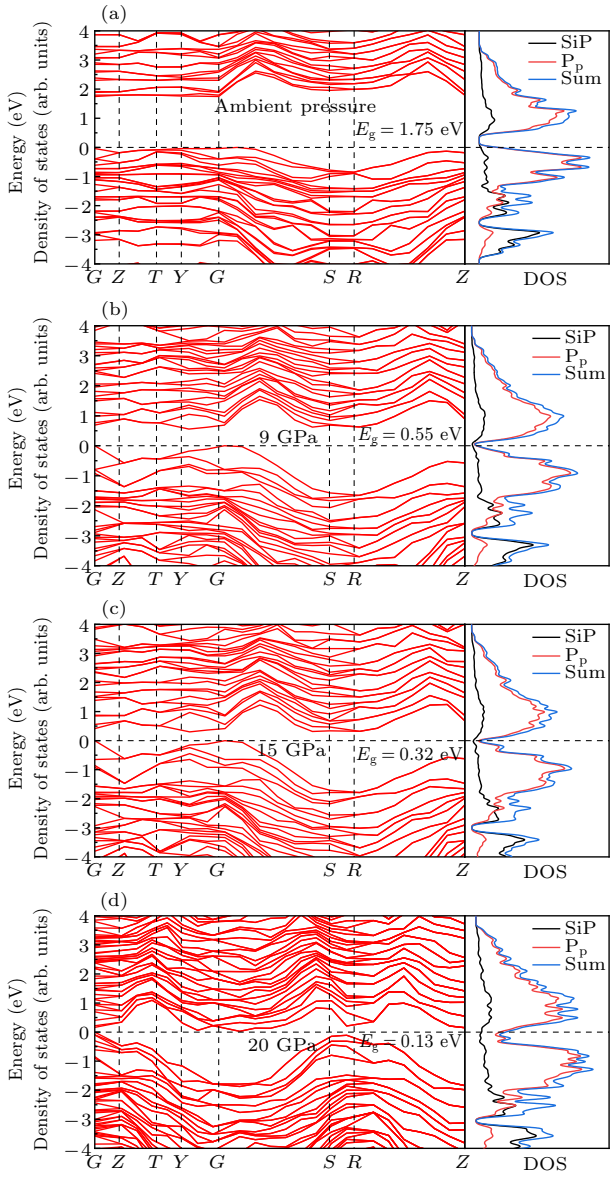


Fig. 7. Theoretical calculation of electronic band structures and density of states (DOS) of multilayered SiP at (a) ambient pressure, (b) 9 GPa, (c) 15 GPa, and (d) 20 GPa.

Theoretical calculations of the band structure and density of states under different pressures are shown in Fig. 7, which reveal significant changes in the electronic properties of SiP under pressure. At room temperature and pressure, SiP exhibits a band gap of 1.75 eV. At approximately 20.0 GPa, the band gap narrows to 0.13 eV. When the imposed pressure goes beyond 20.0 GPa, the bandgap closes, resulting in a transition from a semiconducting to a metallic state driven by a pressure-induced electronic structural transition. With increasing pressure, the out-of-plane anisotropic interactions strengthen, while the interlayer vdW interactions weaken. This results in a gradual reduction of the band gap between the conduction band (CB) and the valence band (VB). The behavior can be further elucidated by combining with the tight-binding theory,[59–61] which posits that stronger atomic interactions enhance the overlap integrals between electron orbitals. This increased orbital overlap broadens the energy bands, thereby narrowing the band gap.

The combined experimental and theoretical results reveal that the semiconductor-to-metal transition in SiP occurs at a pressure, nearly coinciding with the threshold for the crystalline-to-amorphous structural transition. Notably, after decompression, SiP retains its amorphous and metallic properties, suggesting a significant interplay between structural disorder and the electronic metallization process. Additionally, we observed that the metallic state remains stable even after pressure is released, highlighting the importance of the amorphous structure in maintaining the metallic electronic characteristics of SiP. These results enhance our understanding of the mechanisms behind pressure-induced phase transitions and offer new insights into the relationship between the structure and properties of novel materials.

4. Summary and conclusions

In summary, we employed Raman spectroscopy, conductivity measurements, first-principles calculations, high-resolution transmission electron microscope and selected area electron diffraction to investigate the structural and electronic properties of 2D layered semiconductor SiP under high-pressure conditions. Above 6.1 GPa, accompanied by the shifts in Raman peaks, the sample begins to exhibit structural distortions, eventually becoming amorphous at 23.3 GPa. The electronic structure undergoes significant changes around 6.8 GPa and a semiconductor-metal transition occurs at ∼20.5 GPa. Notably, the metastable metallic amorphous SiP obtained under extreme conditions can be retained at ambient conditions. This pressure-induced amorphous metal phase offers new insights into the relationship between structure and properties in 2D layered semiconductors. These findings not only enhance our understanding of pressure-mediated electronic transitions but also highlight potential pathways for designing functional materials suitable for next-generation electronic devices.

Acknowledgements

The authors acknowledge Jieru Pu and Yulei He for their valuable assistance in conducting the experiments. We are also grateful to Professor Gang Jiang for his insightful contributions to the theoretical calculations, which greatly enhanced the understanding of our results. Project supported by the National Natural Science Foundation of China (Grant No. 42150102) and the Sichuan Science and Technology Program (Grant No. 2023NSFSC1910).

References

[1] Coak M J, Son S, Daisenberger D, Hamidov H, Haines C R, Alireza P L, Wildes A R, Liu C, Saxena S S and Park J G 2019 *Npj Quantum Mater.* **4** 38
[2] Kim H S, Haule K and Vanderbilt D 2019 *Phys. Rev. Lett.* **123** 236401
[3] Wang Y, Ying J, Zhou Z, Sun J, Wen T, Zhou Y, Li N, Zhang Q, Han F, Xiao Y, Chow P, Yang W, Struzhkin V V, Zhao Y and Mao H 2018 *Nat. Commun.* **9** 1914
[4] Haines C R S, Coak M J, Wildes A R, Lampronti G I, Liu C, Nahai-Williamson P, Hamidov H, Daisenberger D and Saxena S S 2018 *Phys. Rev. Lett.* **121** 266801
[5] Yang Z, Hao J and Lau S P 2020 *J. Appl. Phys.* **127** 220901
[6] Zhao H, Chen X, Wang G, Qiu Y and Guo L 2019 *2D Mater.* **6** 032002
[7] Li N, Peng J, Zhang P and Yue Y 2023 *Adv. Mater.* **35** 2300067
[8] Wu L, Longo A, Dzade N Y, Sharma A, Hendrix M M, Bol A A, De Leeuw N H, Hensen E J and Hofmann J P 2019 *T. ChemSusChem* **12** 4383
[9] Zhang J, Wu J, Guo H, Chen W, Yuan J, Martinez U, Gupta G, Mohite A, Ajayan P M and Lou J 2017 *Adv. Mater.* **29** 1701955
[10] Chen H 1974 *Acta Metall.* **22** 1505
[11] Debenedetti P G and Stillinger F H 2001 *Nature* **410** 259
[12] Du L, Tian Q, Zheng X, Guo W, Liu W, Zhou Y, Shi F and Xu Q 2022 *Activity Energy Environ. Mater.* **5** 912
[13] Liu H, Chen B Q, Pan Y J, Fu C P, Kankala R K, Wang S B and Chen A Z 2021 *Sci. Technol. Adv. Mater.* **22** 695
[14] Liu W, Xu Q, Cui W, Zhu C and Qi Y 2017 *Angew. Chem. Int. Ed.* **56** 1600
[15] Luo Y, Li Q, Tian Y, Liu Y and Chu K 2022 *J. Mater. Chem. A* **10** 1742
[16] Tse J S 1992 *J. Chem. Phys.* **96** 5482
[17] Tse J S and Klein M L 1990 *J. Chem. Phys.* **92** 3992
[18] Han J, Xu S, Sun J, Fang L and Zhu H 2017 *RSC Adv.* **7** 1357
[19] Pandey K, Garg N, Shanavas K, Sharma S M and Sikka S 2011 *Appl. Phys.* **109** 11
[20] Badro J, Gillet P and Barrat J L 1998 *Europhys. Lett.* **42** 643
[21] Wang Y, Zhu J, Yang W, Wen T, Pravica M, Liu Z, Hou M, Fei Y, Kang L and Lin Z 2016 *Nat. Commun.* **7** 12214
[22] Swamy V, Kuznetsov A, Dubrovinsky L S, McMillan P F, Prakapenka V B, Shen G and Muddle B C 2006 *Phys. Rev. Lett.* **96** 135702
[23] Awasthi A P and Subhash G 2019 *J. Appl. Phys.* **125** 215901
[24] Sar H, Gao J and Yang X 2021 *Sci. Rep.* **11** 6372
[25] Zhang S, Guo S, Huang Y, Zhu Z, Cai B, Xie M, Zhou W and Zeng H 2016 *2D Mater.* **4** 015030
[26] Mortazavi B, Shahrokhi M, Cuniberti G and Zhuang X 2019 *Coatings* **9** 522
[27] Xu Y, Shi Z, Shi X, Zhang K and Zhang H 2019 *Nanoscale* **11** 14491
[28] Li C, Wang S, Zhang X, Jia N, Yu T, Zhu M, Liu D and Tao X 2017 *CrystEngComm* **19** 6986
[29] Chen C, Ding Z, Zhou Y, Yuan Y, Qian N, Wang J, Wang S, Zhou Y, An C and Zhang M 2024 *Sci. China- Phys. Mech. Astron.* **67** 258211
[30] Barreteau C, Michon B, Besnard C and Giannini E 2016 *J. Cryst. Growth* **443** 75
[31] Larson A C and Von Dreele R B 1985 *Rep. LAUR* 86–748 (Los Alamos National Laboratory)
[32] Jayaraman A 1983 *Rev. Mod. Phys.* **55** 65
[33] Mao H, Xu J A and Bell P 1986 *Res. Solid Earth* **91** 4673
[34] Zheng F and Li L J 2024 *Electronics Micron* **187** 103707
[35] Chwang R, Smith B and Crowell C 1974 *Solid-State Electron.* **17** 1217
[36] Ramadan A A, Gould R D and Ashour A 1994 *Thin Solid Films* **239** 272
[37] Hafner J and Kresse G 1997 *Properties of Complex Inorganic Solids* pp. 69–82
[38] Bagayoko D 2014 *AIP Adv.* **4** 127104
[39] Perdew J P, Burke K and Ernzerhof M 1996 *Phys. Rev. Lett.* **77** 3865
[40] Kresse G and Furthmüller J 1996 *Phys. Rev. B* **54** 11169
[41] Kresse G and Hafner J 1993 *Phys. Rev. B* **47** 558
[42] Krukau A V, Vydrov O A, Izmaylov A F and Scuseria G E 2006 *J. Chem. Phys.* **125** 224106
[43] Lee J U, Lee S, Ryoo J H, Kang S, Kim T Y, Kim P, Park C H, Park J G and Cheong H 2016 *Nano Lett.* **16** 7433
[44] Kim K, Lim S Y, Kim J, Lee J U, Lee S, Kim P, Park K, Son S, Park C H and Park J G 2019 *2D Mater.* **6** 041001
[45] Ferrari A C and Robertson J 2004 *Philos. Trans. R. Soc. Lond. Ser. Math. Phys. Eng. Sci.* **362** 2477
[46] Li C, Wang S, Li C, Yu T, Jia N, Qiao J, Zhu M, Liu D and Tao X 2018 *J. Mater. Chem. C* **6** 7219
[47] Xie X, Ding J, Wu B, Zheng H, Li S, Wang C T, He J, Liu Z, Wang J T and Duan J 2023 *Nanoscale* **15** 12388
[48] Machon D, Meersman F, Wilding M, Wilson M and McMillan P 2014 *Prog. Mater. Sci.* **61** 216
[49] Zhao J, Liu H, Ehm L, Dong D, Chen Z and Gu G 2013 *J. Phys. Condens. Matter* **25** 125602
[50] Cheng H, Zhang J, Li Y, Li G and Li X 2017 *J. Appl. Phys.* **121** 225902
[51] Dai L, Zhuang Y, Li H, Wu L, Hu H, Liu K, Yang L and Pu C 2017 *J. Mater. Chem. C* **5** 12157
[52] Zhang M G, Chen L, Feng L, Tuo H H, Zhang Y, Wei Q and Li P F 2023 *Chin. Phys. B* **32** 086101
[53] Hu C, Xu Y, Gong Y, Yang D, Li X and Li Y 2022 *Phys. Chem. Chem. Phys.* **24** 10053
[54] Cheng H, Zhang J, Yu P, Gu C, Ren X, Lin C, Li X, Zhao Y, Wang S and Li Y 2020 *J. Phys. Chem. C* **124** 3421
[55] Gao Y, Liu C, Tian C, Zhu C, Huang X and Cui T 2024 *Chin. Phys. B* **33** 126104
[56] Han S, Duan S, Liu Y X, Wang C, Chen X, Sun H R and Liu X B 2023 *Chin. Phys. B* **32** 016101
[57] Bastard G, Brum J and Ferreira R 1991 *Solid State Physics* **44** 229
[58] Kittel C and McEuen P 2018 *Introduction to solid state physics* (John Wiley & Sons) p. 704
[59] Konschuh S, Gmitra M and Fabian J 2010 *Phys. Rev. B* **82** 245412
[60] Pearce A J, Mariani E and Burkard G 2016 *Phys. Rev. B* **94** 155416
[61] Mogulkoc Y, Modarresi M, Mogulkoc A, Ciftci Y and Alkan B 2017 *J. Phys. Chem. Solids* **111** 458